Incorporation of Microfield Distortion into Rapid Effective Property Design

T. I. Zohdi

Mathematics and Mechanics of Solids 2002 7: 237
DOI: 10.1177/108128602027730

Incorporation of Microfield Distortion into Rapid Effective Property Design

T. I. ZOHDI
Department of Mechanical Engineering, 6195 Etcheverry Hall, University of California, Berkeley, CA 94720-1740

(Received 5 July 2001)

Abstract: It is advantageous to use analytical effective property approximations during the initial stages of the design and development of new multiphase solids. Materials of this class are typified by microscopic second-phase particles suspended in a binding matrix. Such approximate methods are ideal since they require minimal computational effort, thus allowing one to perform rapid analyses for large numbers of multiphase solid combinations controlling parameters like the volume fractions and phase contrasts. Afterwards, when the number of feasible microstructural design combinations has been sufficiently narrowed down, one can perform further in-depth studies, applying computationally intensive numerical simulations, or more involved laboratory tests, to a reduced set of design alternatives. However, a limitation of approximate methods is that they do not provide much quantifiable information about the internal stress and strain fields in the material. Clearly, during material design development, when selecting micro-additives, information about the changes in the otherwise (relatively) smooth internal fields, corresponding to the matrix material alone, would be valuable to characterize a new multiphase material's performance. With regard to materials possessing microstructures described by particles suspended in a binding matrix, one obvious quantity of interest is the microfield distortion, defined as the difference between the fields produced when heterogeneities are present and fields produced when the heterogeneities are absent. Consistent with the use of computationally inexpensive effective property approximations, such information would be attractive, especially if it involved *no extra intensive numerical simulations*. Accordingly, in this work an *exact* expression is derived for the microfield distortion, solely in terms of the external loading, property mismatches and volume fractions. Examples are given illustrating use of the expression in a design setting whereby second-phase additives are sought which deliver desired effective responses, while simultaneously obeying microfield distortion constraints.

Key Words: Inverse problems, irregular heterogeneous microstructure

1. INTRODUCTION

In many modern scientific applications, multiphase materials are now commonly used. In the design of such materials, the basic philosophy is to select material combinations to produce macroscopic responses possessing desirable properties from each component. One relatively common process in manufacturing a certain class of multiphase materials is the vortex method, whereby loose particulate additives are stirred into a vortex of molten matrix material. The resulting microstructure consists of randomly distributed particles suspended in a binding matrix (Figure 1). Mathematically, the mechanical properties of

Mathematics and Mechanics of Solids, **7:** 237–254, 2002 DOI: 10.1177/108128602027730

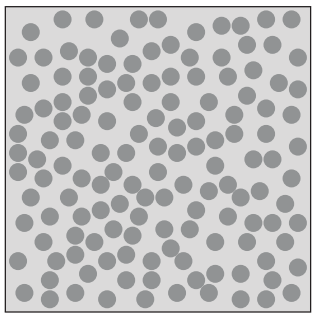

Figure 1. Randomly distributed particles in a binding matrix.

microheterogeneous materials are characterized by a spatially variable elasticity tensor $\mathbb{E}$. Typically, in order to characterize the (homogenized) effective macroscopic response of such materials, a relation between averages $\langle \boldsymbol{\sigma} \rangle_\Omega = \mathbb{E}^* : \langle \boldsymbol{\epsilon} \rangle_\Omega$ is sought, where $\langle \cdot \rangle_\Omega \stackrel{\text{def}}{=} \frac{1}{|\Omega|} \int_\Omega \cdot d\Omega$, and where $\boldsymbol{\sigma}$ and $\boldsymbol{\epsilon}$ are the stress and strain tensor fields within a statistically representative volume element (RVE) of volume $|\Omega|$. The quantity $\mathbb{E}^*$ is known as the effective property, and is the elasticity tensor used in usual structural scale analyses.

For the effective property to be useful, i.e. statistically representative, it must be computed over a sample containing a large amount of material. In other words, the sample must be so large that for further enlargements $\mathbb{E}^*$ does not change. If one were to attempt to perform a direct numerical simulation of a truly statistically representative volume element of material, incorporating all of the microscale details, an extremely fine spatial discretization mesh, for example that of a finite-element mesh, would be required in order to accurately resolve the microstructural fields. In order to give an idea of the immensity of the computational problem, consider that in metals possessing particulate microstructure, a cubical sample of dimensions 0.0001 m$\times 0.0001$ m$\times 0.0001$ m, *which may still not even be statistically representative*, can typically contain of the order of 1000–10,000 particles suspended in a binding matrix. For three-dimensional problems, thousands of numerical degrees of freedom per particle are needed to deliver numerically accurate solutions, and thus the resulting system of equations would contain several million numerical unknowns. Furthermore, while there exist a variety of numerical techniques specifically designed to simulate such problems, for example micromechanical domain decomposition methods originally developed in Huet [1] and recently extended in Zohdi et. al. [2], they are computationally demanding, even when modern computational facilities are available. For reviews see Huet [3] and [4]. Additionally, if inverse problems of material design are of interest, where several hundred or thousand possible microstructural parameter combinations are to be tested, such processes become even more intensive.

In many cases, during material design and development, one would like to perform relatively quick analyses with minimal intensive computational effort, in order to approximately determine new microheterogeneous solid combinations which deliver prespecified desired $\mathbb{E}^*$s. In other words, one would like to rapidly 'narrow down' the number of feasible microstructural combinations, and then perform more in-depth analyses with

numerical simulations over a reduced set of design alternatives afterwards. This is one reason that a variety of analytical effective property approximation techniques, which serve as guides in the selection of material combinations, are frequently used.[1] A variety of approximations, such as the dilute method (based on the results of Eshelby [6]), the Hashin–Shtrikman bounds (Hashin and Shtrikman [7] and [8]), the self-consistent method (Budiansky [9] and Hill [10]) and the Mori–Tanaka method (Mori and Tanaka [11]) have wide continued use in the mechanics community. For a detailed overview, we refer the reader to Nemat-Nasser and Hori [5]. *However, a limitation of such approximate methods is that they do not provide much quantifiable information about the internal stress and strain fields in the material.* Clearly, during material design development, when selecting micro-additives, information about the changes in the otherwise (relatively) smooth internal fields, corresponding to the matrix material alone, would be valuable for characterizing a new multiphase material's performance. With regard to materials possessing microstructures described by particles suspended in a binding matrix, one obvious quantity of interest is the microfield distortion, defined as the difference between the fields produced when heterogeneities are present and fields produced when the heterogeneities are absent. Consistent with the use of computationally inexpensive effective property approximations, such information would be attractive, especially if it involved *no extra intensive numerical computations*. Accordingly, in this work an *exact* expression is derived for such a microscale distortion measure in an induced energy norm. The result is obtained under no assumptions on the character of the microstructure of the material, other than it be pointwise positive-definite, as well as under no assumptions on the external loading and geometry. The expression is solely in terms of easily accessible microstructural data, such as the property mismatches and volume fractions, and thus it introduces no extra significant computational burden. Afterwards, more precise analyses of the responses can be computationally performed, *on a reduced set of feasible designs*, employing large-scale numerical techniques.

The outline of the paper is as follows. In section 2, some background information is given. In section 3, the fundamental structure of a micro–macro objective function, i.e. one specifying a desired macroscopic response while simultaneously satisfying microfield constraints, is discussed. In section 4, an exact expression of the microfield distortion measure is derived. In section 5, numerical examples are given addressing inverse material design problems, whereby second-phase additives are sought to modify a base matrix in order to deliver a desired effective response, while simultaneously obeying microfield distortion constraints. Finally, in section 6, some concluding remarks are given.

2. BACKGROUND INFORMATION

A sample of perfectly bonded heterogeneous material with domain Ω, under a given set of specified boundary loadings, is considered (Figure 1). Its boundary is denoted as $\partial\Omega$. The body is in static equilibrium under the action of body forces, $\mathbf{f}$, and surface tractions, $\mathbf{t}$. The boundary $\overline{\partial\Omega} = \overline{\Gamma_u \cup \Gamma_t}$ consists of a part Γ_u and a part Γ_t on which displacements and tractions are respectively prescribed. Following standard notation, $H^1(\Omega)$ is denoted as the usual space of functions with generalized partial derivatives of order ≤ 1 in $L^2(\Omega)$. The symbol $\mathbf{H}^1(\Omega) \stackrel{\text{def}}{=} [H^1(\Omega)]^3$ is defined as the space of vector-valued functions whose

components have generalized partial derivatives ≤ 1 in $\mathbf{L}^2(\Omega) \stackrel{\text{def}}{=} [L^2(\Omega)]^3$. The data are assumed to be such that $\mathbf{f} \in \mathbf{L}^2(\Omega)$ and $\mathbf{t} \in \mathbf{L}^2(\Gamma_t)$, but less smooth data can be considered without complications. The symbol '$\mathbf{u}|_{\partial\Omega}$' is used for generalized boundary values, for example for specified boundary displacements. Throughout the analysis, the microstructure, which is characterized by $\mathbb{E} \in \mathcal{R}^{3^2 \times 3^2}$ whose components satisfy, $\forall \boldsymbol{\epsilon} \in \mathcal{R}^{3\times 3}$, $\boldsymbol{\epsilon} = \boldsymbol{\epsilon}^T$, $a^- \boldsymbol{\epsilon} : \boldsymbol{\epsilon} \leq \boldsymbol{\epsilon} : \mathbb{E} : \boldsymbol{\epsilon} \leq a^+ \boldsymbol{\epsilon} : \boldsymbol{\epsilon}$, $0 < a^-, a^+ < \infty$, $\forall \mathbf{x} \in \Omega$, where $E_{ijkl} = E_{jikl} = E_{ijlk} = E_{klij}$, $1 \leq i,j,k,l \leq 3$, and where E_{ijkl} are the Cartesian components of $\mathbb{E}$.

A general variational boundary value formulation for the class of problems considered is

$$\text{Find } \mathbf{u} \in \mathbf{H}^1(\Omega), \mathbf{u}|_{\Gamma_u} = \mathbf{d}, \text{ such that}$$

$$\int_\Omega \nabla \mathbf{v} : E : \nabla \mathbf{u} d\Omega = \int_\Omega \mathbf{f} \cdot \mathbf{v} d\Omega + \int_{\Gamma_t} \mathbf{t} \cdot \mathbf{v} dA, \quad \forall \mathbf{v} \in \mathbf{H}^1(\Omega), \mathbf{v}|_{\Gamma_u} = \mathbf{0} \quad (1)$$

When considering a material design process, the boundary value problem in Equation 1 must to be solved for each new microstructure ($\mathbb{E}$). A standard restriction on the types of loading which are consistent with micro–macro scale concepts is Hill's condition, $\langle \boldsymbol{\sigma} : \boldsymbol{\epsilon} \rangle_\Omega = \langle \boldsymbol{\sigma} \rangle_\Omega : \langle \boldsymbol{\epsilon} \rangle_\Omega$. Hill's condition dictates the size requirements on the sample to be statistically representative. In order to see this, consider that for any perfectly bonded heterogeneous body, in the absence of body forces ($\mathbf{f} = \mathbf{0}$), two physically important loading states satisfy Hill's condition: (1) pure linear boundary displacements of the form $\mathbf{u}|_{\partial\Omega} = \mathcal{E} \cdot \mathbf{x}$, where represents a constant applied strain, which implies $\langle \boldsymbol{\epsilon} \rangle_\Omega = \mathcal{E}$; and (2) pure boundary tractions in the form $\mathbf{t}|_{\partial\Omega} = \mathcal{L} \cdot \mathbf{n}$, which implies $\langle \boldsymbol{\sigma} \rangle_\Omega = \mathcal{L}$, where $\mathcal{L}$ represents a constant applied stress tensor. One can thus consider that applying either of the above-mentioned boundary loadings on a large sample of material is a way of approximately generating the boundary conditions on a statistically representative subdomain of heterogeneous material within a macroscopic body. In practice, by applying six linearly independent loadings on a large sample of material of either form (1) or (2), one can determine the components of $\mathbb{E}^*$. If the material is macroscopically isotropic, then only one loading test, containing nonzero dilatational ($\frac{tr\boldsymbol{\sigma}}{3}$ and $\frac{tr\boldsymbol{\epsilon}}{3}$) and deviatoric components ($\boldsymbol{\sigma}' \stackrel{\text{def}}{=} \boldsymbol{\sigma} - \frac{tr\boldsymbol{\sigma}}{3}$ and $\boldsymbol{\epsilon}' \stackrel{\text{def}}{=} \boldsymbol{\epsilon} - \frac{tr\boldsymbol{\epsilon}}{3}$), is necessary to determine the effective bulk and shear moduli: $3\kappa^* \langle \frac{tr\boldsymbol{\epsilon}}{3} \rangle_\Omega = \langle \frac{tr\boldsymbol{\sigma}}{3} \rangle_\Omega$ and $2\mu^* \langle \boldsymbol{\epsilon}' \rangle_\Omega = \langle \boldsymbol{\sigma}' \rangle_\Omega$.

3. THE DESIGN OF AN EFFECTIVE RESPONSE

Consider a one-dimensional bar of length L composed of random particles, i.e. strips in one dimension (Figure 2). There are a total of N strips: N_2 dark strips, each of thickness a, and N_1 white strips representing the rest of the material. The Young's modulus E_2 corresponds to the 'particles', while R corresponds to the 'matrix'. Suppose one wishes to design an effective response, E^*, of such a structure defined by $\langle \sigma \rangle_\Omega = E^* \langle \epsilon \rangle_\Omega$. Consider the following two-point boundary value problem: $\frac{d}{dx}(E\frac{du}{dx}) = 0$, $u(0) = 0$, $u(L) = \mathcal{E} \times L$, where $\mathcal{E}$ is a constant. One finds that

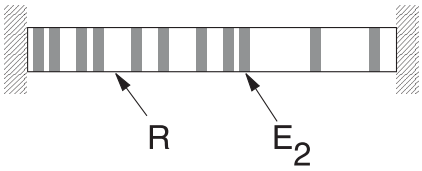

Figure 2. A simple one-dimensional heterogeneous structure.

$$E^* = \frac{\zeta R}{(1-\nu_2)\zeta + \nu_2}, \tag{2}$$

where $\zeta = \frac{E_2}{R}$, $\nu_1 + \nu_2 = 1$ and $\nu_2 = \frac{N_2 a}{L}$. Clearly, there is no unique combination of ζ and ν_2 to produce the same desired effective response.

3.1. Incorporation of microfield constraints

Let us define the (one-dimensional) induced energy norm comparing two strain fields:

$$0 \leq ||u-w||^2_{E(\Omega)} \stackrel{\text{def}}{=} \int_\Omega (\frac{du}{dx} - \frac{dw}{dx}) E (\frac{du}{dx} - \frac{dw}{dx}) d\Omega. \tag{3}$$

Note that in the event that displacements are specified on the boundary, then $u-w =$ constant is unobtainable unless $u = w$, and the semi-norm in Equation (3) is a norm in the strict mathematical sense. Also we define the complementary norm comparing two stress fields:

$$0 \leq ||\sigma - \gamma||^2_{E^{-1}(\Omega)} \stackrel{\text{def}}{=} \int_\Omega (\sigma - \gamma) E^{-1} (\sigma - \gamma) d\Omega. \tag{4}$$

As for the heterogeneous structure, let us consider the same one-dimensional bar, however composed of only the matrix material, R. We consider the following two-point boundary value problem, $\frac{d}{dx}(R\frac{du}{dx}) = 0, u(0) = 0, u(L) = \mathcal{E} \times L$. The stress is simply $\sigma^R = R\mathcal{E}$ and the strain is $\epsilon^R = \mathcal{E}$. Let us define the distortion due to the inhomogeneities as the difference between the fields of the heterogeneous and homogeneous systems:

$$\pi^2 = \frac{||u-u^R||^2_{E(\Omega)} + ||\sigma - \sigma^R||^2_{E^{-1}(\Omega)}}{||u^R||^2_{R(\Omega)} + ||\sigma^R||^2_{R^{-1}(\Omega)}}. \tag{5}$$

Therefore, we can now set up the following system of equations for macroscopic and microscopic design criteria:

$$\begin{aligned} \text{MACROSCOPIC} \quad &: \quad \Pi = E^* = E^{*,D}, \\ \text{MICROSCOPIC} \quad &: \quad \pi^2 = \frac{||u-u^R||^2_{E(\Omega)} + ||\sigma - \sigma^R||^2_{E^{-1}(\Omega)}}{||u^R||^2_{E(\Omega)} + ||\sigma^R||^2_{E^{-1}(\Omega)}} = \delta, \end{aligned} \tag{6}$$

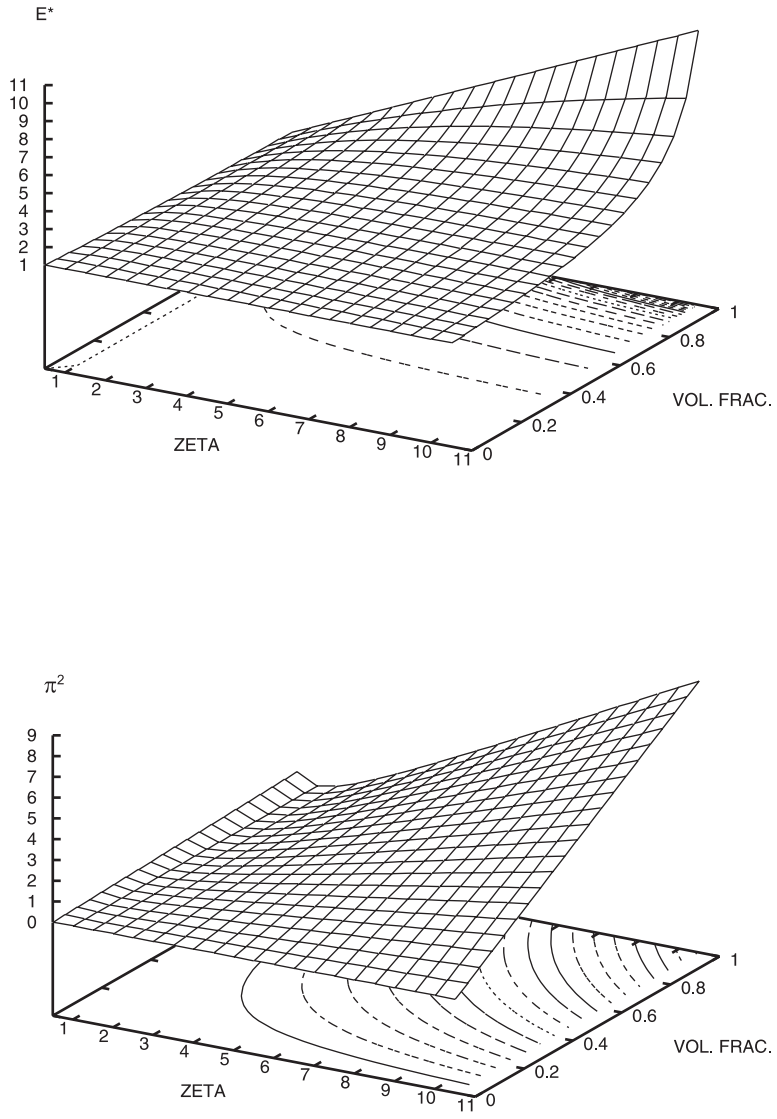

Figure 3. The surfaces for E^* (TOP) and π^2 (BOTTOM) for $1 \leq \zeta$.

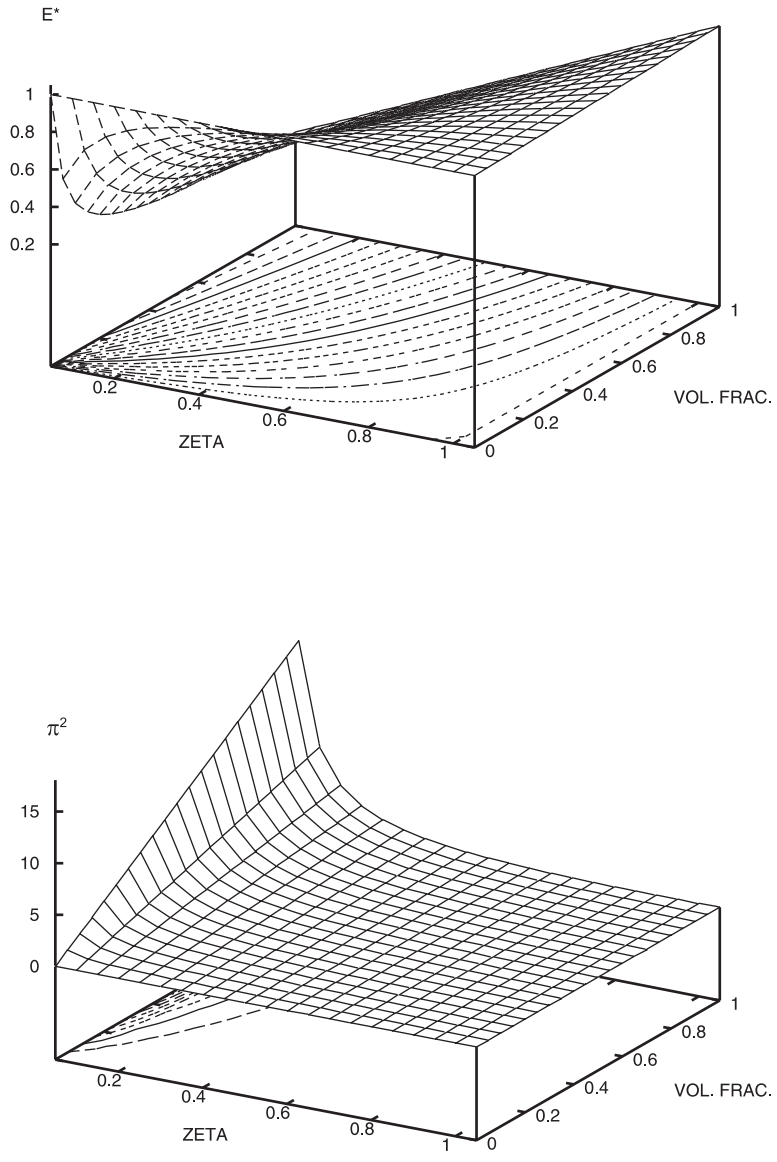

Figure 4. The surfaces for E^* (TOP) and π^2 (BOTTOM) for $0 < \zeta \leq 1$.

where δ is a distortion tolerance on the microfield and where $E^{*,D}$ is a desired effective response. After some algebra, this leads to the following:

$$\zeta = 1 + 2\frac{\delta E^{*,D}}{E^{*,D} - R} \quad \text{and} \quad v_2 = \frac{(E^{*,D} - R)^2 + 2\delta E^{*,D}(E^{*,D} - R)}{2\delta (E^{*,D})^2}. \tag{7}$$

This solution, which is unique, is feasible only if the following restrictions are obeyed:

$$0 < \underbrace{1 + 2\frac{\delta E^{*,D}}{E^{*,D} - R}}_{\zeta} < \infty \quad \text{and} \quad 0 \leq \underbrace{\frac{(E^{*,D} - R)^2 + 2\delta E^{*,D}(E^{*,D} - R)}{2\delta (E^{*,D})^2}}_{v_2} \leq 1. \tag{8}$$

Clearly, the macroscopic and microscopic objectives cannot always be met simultaneously, i.e. in some cases no feasible solutions exist. This is graphically illustrated by the surfaces of $\mathbb{E}^*$ and π^2 (Figures 3 and 4), which may or may not intersect. This depends on the desired objectives $E^{*,D}$ and δ. We denote the formulation of prespecifying a macroscopic response with microfield constraints as a *micro–macro design problem*.

3.2. Preface to three-dimensional analyses

Unlike in the simple one-dimensional example, for three-dimensional problems involving a statistically representative sample of material, the microfields cannot be determined pointwise analytically, and then simply post-processed to determine $\mathbb{E}^*$ and π^2. *Consistent with the premise that one would like to (initially) avoid intensive numerical simulations, one must resort to estimates of* $\mathbb{E}^*$. The simplest estimates are the Hill–Reuss–Voigt bounds [12], [14], [13]: $\langle \mathbb{E}^{-1} \rangle_\Omega^{-1} \leq \mathbb{E}^* \leq \langle \mathbb{E} \rangle_\Omega$. The notation means that the difference tensors $(\langle \mathbb{E} \rangle_\Omega - \mathbb{E}^*)$ and $(\mathbb{E}^* - \langle \mathbb{E}^{-1} \rangle_\Omega^{-1})$ are positive-definite. For isotropic macroscopic responses with isotropic phases this implies $\langle \kappa^{-1} \rangle_\Omega^{-1} \leq \kappa^* \leq \langle \kappa \rangle_\Omega$ and $\langle \mu^{-1} \rangle_\Omega^{-1} \leq \mu^* \leq \langle \mu \rangle_\Omega$, where κ and μ are the spatially variable bulk and shear moduli of material. In 1963, such bounds were improved by Hashin and Shtrikman [7], [8], for isotropic materials with an isotropic effective response, resulting in the following:

$$\underbrace{\kappa_1 + \frac{v_2}{\frac{1}{\kappa_2 - \kappa_1} + \frac{3(1-v_2)}{3\kappa_1 + 4\mu_1}}}_{\text{bulk modulus H/S lower bound}} \leq \kappa^* \leq \underbrace{\kappa_2 + \frac{1 - v_2}{\frac{1}{\kappa_1 - \kappa_2} + \frac{3v_2}{3\kappa_2 + 4\mu_2}}}_{\text{bulk modulus H/S upper bound}}, \tag{9}$$

and

$$\underbrace{\mu_1 + \frac{v_2}{\frac{1}{\mu_2 - \mu_1} + \frac{6(1-v_2)(\kappa_1 + 2\mu_1)}{5\mu_1(3\kappa_1 + 4\mu_1)}}}_{\text{shear modulus H/S lower bound}} \leq \mu^* \leq \underbrace{\mu_2 + \frac{(1 - v_2)}{\frac{1}{\mu_1 - \mu_2} + \frac{6v_2(\kappa_2 + 2\mu_2)}{5\mu_2(3\kappa_2 + 4\mu_2)}}}_{\text{shear modulus H/S upper bound}} \tag{10}$$

where κ_1, μ_1 and κ_2, μ_2 are the bulk and shear moduli for the phases, while v_2 is the second-phase volume fraction. Such bounds are the tightest possible on isotropic effective responses, with isotropic two-phase microstructures, where only the volume fractions and

phase contrasts of the constituents are known. For soft-matrix/hard-particle combinations, the Hashin–Shtrikman lower bounds are known to give good estimates for the effective moduli, while for the effective moduli of hard-matrix/soft-particle combinations the Hashin–Shtrikman upper bounds are appropriate. In this work, the Hashin–Shtrikman bounds will be used to approximate the effective responses. However, with regard to being able to set up a tractable micro–macro design formulation, this still leaves open the question of the characterization of π^2. *Surprisingly,* π^2 *can be determined exactly with knowledge of just* $\mathbf{u}^R$, $\mathbb{R}$ *and* $\mathbb{E}$*, using potential theory.*

4. MICROFIELD DISTORTION/A POTENTIAL RESIDUAL

Two boundary value problems are considered, one where the mechanical properties of the material are characterized by a (regular) spatially constant admissible inhomogeneity-free elasticity tensor, $\mathbb{R}$, and another with an admissible spatially nonconstant (inhomogeneous) elasticity tensor, $\mathbb{E}$.

4.1. Homogeneous coefficient boundary value problem

The solution to the constant-coefficient problem, denoted the *regular* solution, $\mathbf{u}^R$, is characterized by a virtual work formulation:

$$\text{Find a } \mathbf{u}^R \in \mathbf{H}^1(\Omega), \mathbf{u}^R|_{\Gamma_u} = \mathbf{d}, \text{ such that}$$

$$\underbrace{\int_\Omega \nabla \mathbf{v} : \boldsymbol{\sigma}^R \, D\Omega}_{\stackrel{\text{def}}{=} \mathcal{B}^R(\mathbf{u}^R, \mathbf{v})} = \underbrace{\int_\Omega \mathbf{f} \cdot \mathbf{v} d\Omega + \int_{\Gamma_t} \mathbf{t} \cdot \mathbf{v} dA}_{\stackrel{\text{def}}{=} \mathcal{F}(\mathbf{v})} \quad \forall \mathbf{v} \in \mathbf{H}^1(\Omega), \mathbf{v}|_{\Gamma_u} = \mathbf{0}, \tag{11}$$

where $\boldsymbol{\sigma}^R = \mathbb{R} : \nabla \mathbf{u}^R$. The equivalent complementary form is

$$\text{Find } \boldsymbol{\sigma}^R, \nabla \cdot \boldsymbol{\sigma}^R + \mathbf{f} = \mathbf{0}, \boldsymbol{\sigma}^R \cdot \mathbf{n}|_{\Gamma_t} = \mathbf{t} \text{ such that}$$

$$\underbrace{\int_\Omega \boldsymbol{\tau} : \mathbb{R}^{-1} : \boldsymbol{\sigma}^R \, d\Omega}_{\stackrel{\text{def}}{=} \mathcal{A}^R(\boldsymbol{\sigma}^R, \boldsymbol{\tau})} = \underbrace{\int_{\Gamma_u} \boldsymbol{\tau} \cdot \mathbf{n} \cdot \mathbf{d} dA}_{\stackrel{\text{def}}{=} \mathcal{G}(\boldsymbol{\tau})} \quad \forall \boldsymbol{\tau}, \nabla \cdot \boldsymbol{\tau} = \mathbf{0}, \boldsymbol{\tau} \cdot \mathbf{n}|_{\Gamma_t} = \mathbf{0}. \tag{12}$$

For the complementary problem, similar restrictions are placed on the solution and test fields to force the integrals to make sense. In other words, we assume that solutions produce finite global energy.

4.2. Inhomogeneous coefficient boundary value problem

The solution corresponding to a material with microstructure is $\mathbf{u}$, and is characterized by the following virtual work formulation:

$$\text{Find } \mathbf{u} \in \mathbf{H}^1(\Omega), \mathbf{u}|_{\Gamma_u} = \mathbf{d}, \text{ such that}$$

$$\underbrace{\int_\Omega \nabla \mathbf{v} : \boldsymbol{\sigma} d\Omega}_{\stackrel{\text{def}}{=} \mathcal{B}^R(\mathbf{u},\mathbf{v})} = \underbrace{\int_\Omega \mathbf{f}\cdot\mathbf{v} d\Omega + \int_{\Gamma_t} \mathbf{t}\cdot\mathbf{t} dA}_{\stackrel{\text{def}}{=} \mathcal{F}(\mathbf{v})} \quad \forall \mathbf{v} \in \mathbf{H}^1(\Omega)\mathbf{v}|_{\Gamma_u} = \mathbf{0}, \quad (13)$$

where $\boldsymbol{\sigma} = \mathbb{E} : \nabla \mathbf{u}$. The equivalent complementary form is

$$\text{Find } \boldsymbol{\sigma}, \nabla\cdot\boldsymbol{\sigma} + \mathbf{f} = \mathbf{0}, \boldsymbol{\sigma}\cdot\mathbf{n}|_{\Gamma_t} = \mathbf{t} \text{ such that}$$

$$\underbrace{\int_\Omega \boldsymbol{\tau} : \mathbb{E}^{-1} : \boldsymbol{\sigma} d\Omega}_{\stackrel{\text{def}}{=} \mathcal{A}(\boldsymbol{\sigma},\boldsymbol{\tau})} = \underbrace{\int_{\Gamma_u} \boldsymbol{\tau}\cdot\mathbf{n}\cdot\mathbf{d} dA}_{\stackrel{\text{def}}{=} \mathcal{G}(\boldsymbol{\tau})} \quad \forall \boldsymbol{\tau}, \nabla\cdot\boldsymbol{\tau} = \mathbf{0}, \boldsymbol{\tau}\cdot\mathbf{n}|_{\Gamma_t} = \mathbf{0}. \quad (14)$$

4.3. A potential residual

We have for any kinematically admissible function $\mathbf{w}$, a natural definition of the induced primal energy norm:

$$0 \leq ||\mathbf{u}-\mathbf{w}||^2_{E(\Omega)} \stackrel{\text{def}}{=} \underbrace{\int_\Omega (\nabla\mathbf{u} - \nabla\mathbf{w}) : \mathbb{E} : (\nabla\mathbf{u} - \nabla\mathbf{w}) d\Omega}_{\mathcal{B}(\mathbf{u}-\mathbf{w},\mathbf{u}-\mathbf{w})} . \quad (15)$$

We may write

$$\begin{aligned}
0 \leq ||\mathbf{u}-\mathbf{w}||^2_{E(\Omega)} &= \mathcal{B}(\mathbf{u}-\mathbf{w},\mathbf{u}-\mathbf{w}) \\
&= \mathcal{B}(\mathbf{u},\mathbf{u}) + \mathcal{B}(\mathbf{w},\mathbf{w}) - 2\mathcal{B}(\mathbf{u},\mathbf{w}) \\
&= \mathcal{B}(\mathbf{w},\mathbf{w}) - \mathcal{B}(\mathbf{u},\mathbf{u}) - 2\mathcal{B}(\mathbf{u},\mathbf{w}) + 2\mathcal{B}(\mathbf{u},\mathbf{u}) \\
&= \mathcal{B}(\mathbf{w},\mathbf{w}) - \mathcal{B}(\mathbf{u},\mathbf{u}) - 2\mathcal{B}(\mathbf{u},\mathbf{w}-\mathbf{u}) \\
&= \mathcal{B}(\mathbf{w},\mathbf{w}) - \mathcal{B}(\mathbf{u},\mathbf{u}) - 2\mathcal{F}(\mathbf{w}-\mathbf{u}) \\
&= \mathcal{B}(\mathbf{w},\mathbf{w}) - 2\mathcal{F}(\mathbf{w}) - (\mathcal{B}(\mathbf{u},\mathbf{u}) - 2\mathcal{F}(\mathbf{u})) \\
&= 2\mathcal{J}(\mathbf{w}) - 2\mathcal{J}(\mathbf{u}), \quad (16)
\end{aligned}$$

where we define the elastic potential as $\mathcal{J}(\mathbf{w}) \stackrel{\text{def}}{=} \frac{1}{2}\mathcal{B}(\mathbf{w},\mathbf{w}) - \mathcal{F}(\mathbf{w}) = \frac{1}{2}\int_\Omega \nabla\mathbf{w} : \mathbb{E} : \nabla\mathbf{w} d\Omega - \int_\Omega \mathbf{f}\cdot\mathbf{w} d\Omega - \int_{\Gamma_t} \mathbf{t}\cdot\mathbf{w}$. Clearly, the true solution possesses the minimum potential, which is a restatement of the principle of minimum potential energy. Similarly, for the complementary variational formulation, for any statically admissible function ($\boldsymbol{\gamma}$), one has for the induced complementary energy norm

$$\begin{aligned}
0 \le ||\boldsymbol{\sigma}-\boldsymbol{\gamma}||^2_{E^{-1}(\Omega)} &= \mathcal{A}(\boldsymbol{\sigma}-\boldsymbol{\gamma},\boldsymbol{\sigma}-\boldsymbol{\gamma}) \\
&= \mathcal{A}(\boldsymbol{\sigma},\boldsymbol{\sigma}) + \mathcal{A}(\boldsymbol{\gamma},\boldsymbol{\gamma}) - 2\mathcal{A}(\boldsymbol{\sigma},\boldsymbol{\gamma}) \\
&= \mathcal{A}(\boldsymbol{\gamma},\boldsymbol{\gamma}) - \mathcal{A}(\boldsymbol{\sigma},\boldsymbol{\sigma}) - 2\mathcal{A}(\boldsymbol{\sigma},\boldsymbol{\gamma}) + 2\mathcal{A}(\boldsymbol{\sigma},\boldsymbol{\sigma}) \\
&= \mathcal{A}(\boldsymbol{\gamma},\boldsymbol{\gamma}) - \mathcal{A}(\boldsymbol{\sigma},\boldsymbol{\sigma}) - 2\mathcal{A}(\boldsymbol{\sigma},\boldsymbol{\gamma}-\boldsymbol{\sigma}) \\
&= \mathcal{A}(\boldsymbol{\gamma},\boldsymbol{\gamma}) - \mathcal{A}(\boldsymbol{\sigma},\boldsymbol{\sigma}) - 2\mathcal{G}(\boldsymbol{\gamma}-\boldsymbol{\sigma}) \\
&= \mathcal{A}(\boldsymbol{\gamma},\boldsymbol{\gamma}) - 2\mathcal{G}(\boldsymbol{\gamma}) - (\mathcal{A}(\boldsymbol{\sigma},\boldsymbol{\sigma}) - 2\mathcal{G}(\boldsymbol{\sigma})) \\
&= 2\mathcal{K}(\boldsymbol{\gamma}) - 2\mathcal{K}(\boldsymbol{\sigma}), \qquad (17)
\end{aligned}$$

where we define $\mathcal{K}(\boldsymbol{\gamma}) \stackrel{\text{def}}{=} \frac{1}{2}\mathcal{A}(\boldsymbol{\gamma},\boldsymbol{\gamma}) - \mathcal{G}(\boldsymbol{\gamma}) = \frac{1}{2}\int_\Omega \boldsymbol{\gamma} : \mathbb{E}^{-1} : \boldsymbol{\gamma} d\Omega - \int_{\Gamma_u} \boldsymbol{\gamma}\cdot\mathbf{n}\cdot\mathbf{d} dA$, which is a form of the principle of minimum complementary potential energy. By adding together the potential energy and the complementary energy we obtain an equation of balance, $\mathcal{J}(\mathbf{u}) + \mathcal{K}(\boldsymbol{\sigma}) = 0$. If we choose $\mathbf{w} = \mathbf{u}^R$, which is a kinematically admissible function, we obtain $||\mathbf{u}-\mathbf{u}^R||^2_{E(\Omega)} = 2(\mathcal{J}(\mathbf{u}^R) - \mathcal{J}(\mathbf{u}))$. Also, choosing $\boldsymbol{\gamma} = \boldsymbol{\sigma}^R$, which is statically admissible, we have $||\boldsymbol{\sigma}-\boldsymbol{\sigma}^R||^2_{E^{-1}(\Omega)} = 2(\mathcal{K}(\boldsymbol{\sigma}^R) - \mathcal{K}(\boldsymbol{\sigma}))$. Combining the two previous results yields

$$2(\mathcal{J}(\mathbf{u}^R) + \mathcal{K}(\boldsymbol{\sigma}^R)) = ||\mathbf{u}-\mathbf{u}^R||^2_{E(\Omega)} + ||\boldsymbol{\sigma}-\boldsymbol{\sigma}^R||^2_{E^{-1}(\Omega)}. \qquad (18)$$

A corresponding normalized measure is

$$\pi^2 \stackrel{\text{def}}{=} \frac{2(\mathcal{J}(\mathbf{u}^R) + \mathcal{K}(\boldsymbol{\sigma}^R))}{||\mathbf{u}^R||^2_{R(\Omega)} + ||\boldsymbol{\sigma}^R||^2_{R^{-1}(\Omega)}} = \frac{||\mathbf{u}-\mathbf{u}^R||^2_{E(\Omega)} + ||\boldsymbol{\sigma}-\boldsymbol{\sigma}^R||^2_{E^{-1}(\Omega)}}{||\mathbf{u}^R||^2_{R(\Omega)} + ||\boldsymbol{\sigma}^R||^2_{R^{-1}(\Omega)}}. \qquad (19)$$

We refer to π^2 as the *potential residual*. The relation in Box 19 allows us, for a given boundary value problem, to exactly determine the differences between solutions produced with a regularized constitutive law, and the exact constitutive law, and requires *no computation of the exact microfield boundary valueproblem*.

Remark. In the previous analyses, the tensor $\mathbb{R}$ could have been nonconstant without altering the results. Related further analyses can be found in Zohdi [15].

4.4. Compact forms

If we consider the case of a microstructure composed of a matrix ($\mathbb{R}$) embedded with particulate matter, under uniform loadings, π^2 attains very compact forms. Under pure linear boundary displacements of the form $\mathbf{u}|_{\partial\Omega} = \mathcal{E} \cdot x$, one has

$$\pi^2 = v_2 \left(\frac{\mathcal{E} : \left(\mathbb{E}_2 + \mathbb{R} : \mathbb{E}_2^{-1} : \mathbb{R} \right) : \mathcal{E}}{2\mathcal{E} : \mathbb{R} : \mathcal{E}} - 1 \right), \tag{20}$$

while under pure boundary tractions in the form $\mathbf{t}|_{\partial\Omega} = \mathcal{L} \cdot \mathbf{n}$,

$$\pi^2 = v_2 \left(\frac{\mathcal{L} : \left(\mathbb{E}_2^{-1} + \mathbb{R}^{-1} : \mathbb{E}_2 : \mathbb{R}^{-1} \right) : \mathcal{L}}{2\mathcal{L} : \mathbb{R}^{-1} : \mathcal{L}} - 1 \right), \tag{21}$$

where $\mathcal{E}$ and $\mathcal{L}$ are the (boundary) constant strain and stress tensors introduced earlier. One immediately notices that Boxes 20 and 21 depend only on the external loading, the volume fractions and the mechanical properties of the constituents, thus making either expression trivial to compute. If $\mathcal{L} = \mathbb{R} : \mathcal{E}$, then the forms in Boxes 20 and 21 are equivalent. Clearly, under uniform boundary loading, π^2 is linear in terms of v_2. The dependence of π^2 on the mechanical properties is less obvious due to the presence of two 'competing' terms, $\mathbb{E}_2$ and $\mathbb{E}_2^{-1}$. In order to clearly see the inherent structure of π^2, consider the special case when the elasticity tensor of the stiffness of the particulate material is a uniform scaling of the matrix material, $\mathbb{E} = \zeta \mathbb{R}$ where $\zeta = 1$ in the matrix, and where $\zeta \neq 1$ in the particles ($0 < \zeta < \infty$). Under these conditions, Boxes 20 and 21 collapse to

$$\pi^2 = \frac{v_2}{2} \left(\sqrt{\zeta} - \frac{1}{\sqrt{\zeta}} \right)^2 = \frac{v_2}{2} \left(\zeta - 2 + \frac{1}{\zeta} \right). \tag{22}$$

Clearly, as $\zeta \to \infty$, then $\pi^2 \to \infty$ linearly in ζ, while as $\zeta \to 0$ then $\pi^2 \to \infty$ as $\frac{1}{\zeta}$. In either case, the microfield distortion increases monotonically as the mismatch deviates from unity. The results imply, for heterogeneous materials with the same scaling for the bulk and shear components of the second-phase particles, that soft particles in a hard matrix produce more *overall* distortion than hard particles in a soft matrix, due to the faster growth of $\frac{1}{\zeta}$, relative to that of ζ, in π^2.

5. EXAMPLES WITH MICRO MACRO OBJECTIVES

We consider examples with isotropic macroscopic objectives of the form $\kappa^* = \kappa^{*,D}$ and $\mu^* = \mu^{*,D}$ and a microscopic objective of $\pi^2 = \delta$. This corresponds to specifying a desired macroscopic isotropic behavior of the material, while simultaneously achieving a certain internal distortion level. For purposes of realistic numerical experiment, we chose $\kappa_1 = 77.9$ GPa and $\mu_1 = 24.9$ GPa, which corresponds to a commonly used metal matrix

material (aluminum 6061). Three microstructural design variables are considered: κ_2, μ_2 and v_2. Uniform loading is considered with $\mathcal{L} = \mathbb{R} : \mathcal{E}$, thus making the potential residual equivalent for displacement or traction loading (Equations 20 and 21). As mentioned above, without loss of generality, the Hashin–Shtrikman bounds will be used to approximate the effective responses.[2] We consider two design scenarios:

- CASE I. A model problem of a material with a relatively soft matrix, whose overall stiffness we wish to increase with harder particles. In this case it is appropriate to use the Hashin–Shtrikman lower bounds to characterize the macroscopic responses, since they are known to give reasonable estimates for the effective moduli of soft-matrix/hard-particle combinations. The nonlinear system of coupled equations is

$$\begin{aligned}
\Pi_1 &= \frac{\kappa^*}{\kappa^{*,D}} - 1 = \frac{\kappa_1 + \frac{v_2}{\frac{1}{\kappa_2 - \kappa_1} + \frac{3(1-v_2)}{3\kappa_1 + 4\mu_1}}}{\kappa^{*,D}} - 1 = 0, \\
\Pi_2 &= \frac{\mu^*}{\mu^{*,D}} - 1 = \frac{\mu_1 + \frac{v_2}{\frac{1}{\mu_2 - \mu_1} + \frac{6(1-v_2)(\kappa_1 + 2\mu_1)}{5\mu_1(3\kappa_1 + 4\mu_1)}}}{\mu^{*,D}} - 1 = 0, \qquad (23) \\
\Pi_3 &= \pi^2 - \delta = \frac{2(\mathcal{J}(\mathbf{u}^R) + \mathcal{K}(\boldsymbol{\sigma}^R))}{||\mathbf{u}^R||^2_{R(\Omega)} + ||\boldsymbol{\sigma}^R||^2_{R^{-1}(\Omega)}} - \delta = 0.
\end{aligned}$$

- CASE II. For a model problem of a material with a relatively hard matrix, whose overall stiffness we wish to reduce with softer particles, we employ the Hashin–Shtrikman upper bounds to characterize the macroscopic responses, with the resulting set of equations being

$$\begin{aligned}
\Pi_1 &= \frac{\kappa^*}{\kappa^{*,D}} - 1 = \frac{\kappa_2 + \frac{1-v_2}{\frac{1}{\kappa_1 - \kappa_2} + \frac{3v_2}{3\kappa_2 + 4\mu_2}}}{\kappa^{*,D}} - 1 = 0, \\
\Pi_2 &= \frac{\mu^*}{\mu^{*,D}} - 1 = \frac{\mu_2 + \frac{(1-v_2)}{\frac{1}{\mu_1 - \mu_2} + \frac{6v_2(\kappa_2 + 2\mu_2)}{5\mu_2(3\kappa_2 + 4\mu_2)}}}{\mu^{*,D}} - 1 = 0, \qquad (24) \\
\Pi_3 &= \pi^2 - \delta = \frac{2(\mathcal{J}(\mathbf{u}^R) + \mathcal{K}(\boldsymbol{\sigma}^R))}{||\mathbf{u}^R||^2_{R(\Omega)} + ||\boldsymbol{\sigma}^R||^2_{R^{-1}(\Omega)}} - \delta = 0.
\end{aligned}$$

In either case, the resulting system is solved for by Newton's method. At each Newton iteration, we have three equations and three unknown design increments:

$$\underbrace{\begin{bmatrix} \frac{\partial \Pi_1}{\partial \kappa_2} & \frac{\partial \Pi_1}{\partial \mu_2} & \frac{\partial \Pi_1}{\partial v_2} \\ \frac{\partial \Pi_2}{\partial \kappa_2} & \frac{\partial \Pi_2}{\partial \mu_2} & \frac{\partial \Pi_2}{\partial v_2} \\ \frac{\partial \Pi_3}{\partial \kappa_2} & \frac{\partial \Pi_3}{\partial \mu_2} & \frac{\partial \Pi_3}{\partial v_2} \end{bmatrix}}_{\text{evaluated at previous iteration}} \begin{Bmatrix} \Delta\kappa_2 \\ \Delta\mu_2 \\ \Delta v_2 \end{Bmatrix} = \underbrace{\begin{Bmatrix} -\Pi_1 \\ -\Pi_2 \\ -\Pi_3 \end{Bmatrix}}_{\text{previous values}}, \qquad (25)$$

Table 1. Feasible microstructural solutions for CASE I for a resolution of $50 \times 50 \times 50$ divisions of the desired microdesign space ($\kappa_1 = 77.9$ GPa and $\mu_1 = 24.9$ GPa). Note: for each row, $\frac{\kappa^{*,D}}{\kappa_1}$, $\frac{\mu^{*,D}}{\mu_1}$ and δ were specified, and $\frac{\kappa_2}{\kappa_1}$, $\frac{\mu_2}{\mu_1}$ and v_2 were determined. In each case κ_1 and μ_1 were fixed.

$\frac{\kappa^{*,D}}{\kappa_1}$	$\frac{\mu^{*,D}}{\mu_1}$	δ	$\frac{\kappa_2}{\kappa_1}$	$\frac{\mu_2}{\mu_1}$	v_2	Newton iterations
1.2000	1.6000	.0600	1.4836	2.7404	.4862	39
1.2000	1.8000	.0800	1.4860	3.7103	.4844	21
1.4000	1.2000	.1600	2.3310	1.4943	.4546	98
1.4000	1.6000	.1600	2.1355	2.6855	.4950	67
1.4000	1.8000	.1800	2.1440	3.6072	.4929	39
1.4000	2.2000	.2600	2.1909	7.0863	.4822	18
1.6000	1.2000	.3400	3.2114	1.4532	.4882	28
1.6000	1.6000	.3800	3.3352	2.7937	.4781	23
1.6000	2.0000	.4000	3.1583	4.8414	.4929	27
1.6000	2.0000	.4200	3.2755	5.0709	.4829	35
1.6000	2.0000	.4400	3.3929	5.3029	.4738	17
1.6000	2.2000	.4600	3.2570	6.9832	.4844	25
1.8000	1.2000	.6600	4.6892	1.4408	.4996	29
1.8000	1.4000	.6800	4.7593	1.9882	.4970	20
1.8000	1.4000	.7000	4.8787	2.0005	.4929	21
1.8000	1.4000	.7200	4.9983	2.0123	.4889	20
1.8000	1.4000	.7400	5.1180	2.0237	.4852	12
1.8000	1.4000	.7800	5.3577	2.0453	.4784	15
1.8000	1.4000	.8800	5.9586	2.0934	.4642	19
1.8000	1.6000	.6800	4.6824	2.6564	.4999	17
1.8000	1.6000	.7000	4.8007	2.6820	.4956	18
1.8000	1.6000	.7200	4.9191	2.7067	.4915	19
1.8000	1.6000	.7400	5.0377	2.7308	.4877	21
1.8000	1.6000	.7600	5.1564	2.7541	.4841	14
1.8000	1.8000	.7000	4.6921	3.5328	.4995	14
1.8000	1.8000	.7200	4.8083	3.5799	.4953	13
1.8000	1.8000	.7400	4.9246	3.6260	.4913	14
1.8000	1.8000	.7600	5.0412	3.6710	.4876	15
1.8000	1.8000	.7800	5.1579	3.7150	.4840	15
1.8000	1.8000	.8000	5.2748	3.7580	.4806	17
1.8000	1.8000	.8200	5.3919	3.8001	.4775	19
1.8000	1.8000	.8800	5.7440	3.9208	.4688	27
1.8000	2.0000	.7400	4.7713	4.7636	.4966	13
1.8000	2.0000	.7600	4.8837	4.8465	.4927	15
1.8000	2.2000	.7800	4.7792	6.4774	.4963	13
1.8000	2.2000	.8000	4.8843	6.6231	.4927	15
1.8000	2.4000	.8200	4.6864	8.8449	.4997	16
1.8000	2.4000	.8400	4.7783	9.0962	.4964	17
1.8000	2.4000	.8600	4.8700	9.3503	.4932	18
1.8000	2.4000	.8800	4.9614	9.6072	.4901	17

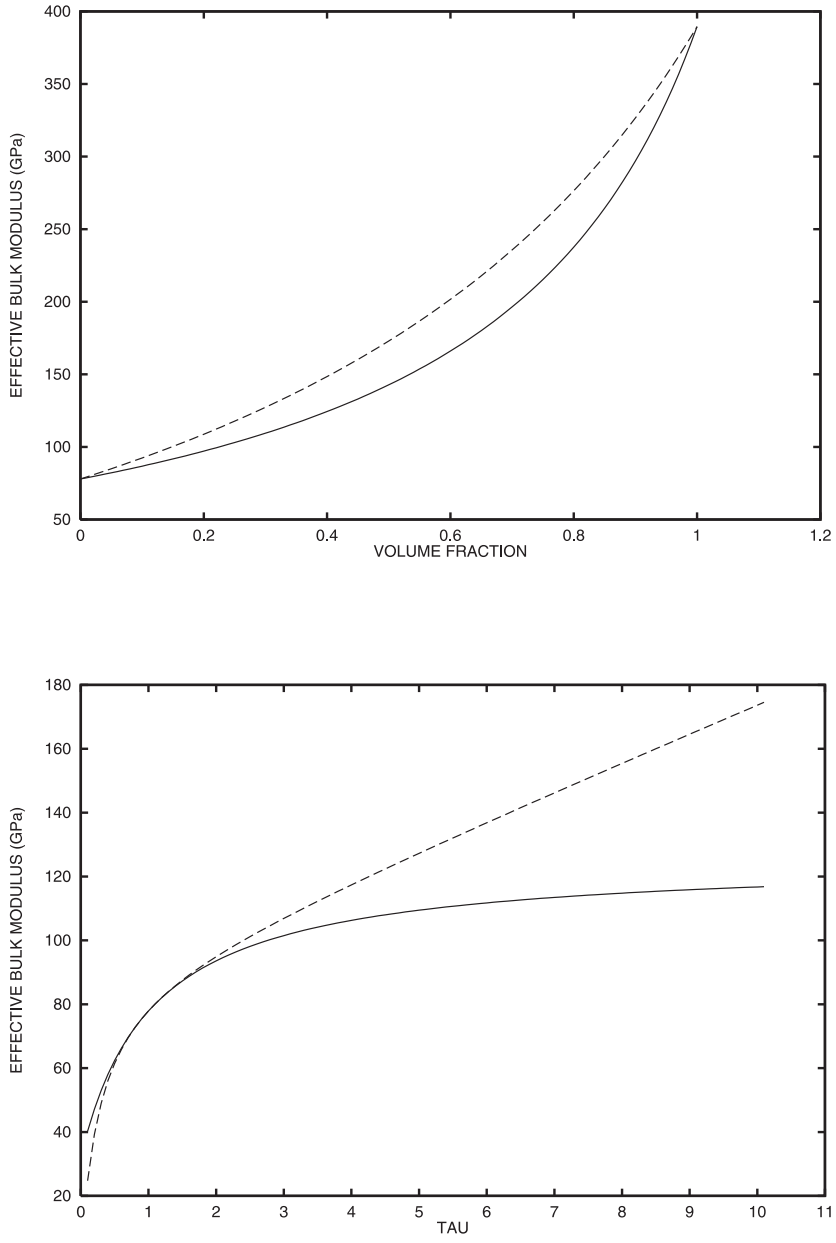

Figure 5. The Hashin–Shtrikman bounds for the effective bulk modulus. TOP: $\zeta = 5$ and variation of the volume fraction. BOTTOM: $v_2 = 0.3$ and variation of ζ, $\kappa_2 = \zeta\kappa_1$ and $\mu_2 = \zeta\mu_1$. The curves are qualitatively similar for the shear modulus.

Table 2. Feasible microstructural solutions for CASE II for a resolution of $50 \times 50 \times 50$ divisions of the desired microdesign space ($\kappa_1 = 77.9$ GPa and $\mu_1 = 24.9$ GPa). Note: for each row, $\frac{\kappa^{*,D}}{\kappa_1}$, $\frac{\mu^{*,D}}{\mu_1}$ and δ were specified, and $\frac{\kappa_2}{\kappa_1}$, $\frac{\mu_2}{\mu_1}$ and v_2 were determined. In each case κ_1 and μ_1 were fixed.

$\frac{\kappa^{*,D}}{\kappa_1}$	$\frac{\mu^{*,D}}{\mu_1}$	δ	$\frac{\kappa_2}{\kappa_1}$	$\frac{\mu_2}{\mu_1}$	v_2	Newton iterations
.8600	.1000	.7400	.7367	.0282	.4566	39
.9000	.1400	.5000	.7953	.0384	.4327	26
.9000	.5800	.0400	.8080	.3311	.4747	47
.9200	.4600	.0800	.8126	.1701	.3807	30
.9400	.1800	.4400	.7844	.0241	.2328	91
.9400	.2800	.2200	.8249	.0586	.3019	33
.9400	.3000	.1800	.8528	.0835	.3713	27
.9400	.5000	.0600	.8622	.2107	.4023	24
.9600	.0800	.9200	.9193	.0232	.4748	18
.9600	.2400	.2200	.9208	.0871	.4853	28
.9600	.4600	.0800	.8906	.1491	.3409	19
.9600	.5000	.0600	.9013	.1988	.3825	13
.9600	.5400	.0400	.9197	.2932	.4797	12
.9800	.0800	.9600	.9545	.0202	.4284	12
.9800	.2200	.3000	.9414	.0469	.3284	18
.9800	.2200	.3200	.9296	.0369	.2696	17
.9800	.2200	.3600	.8849	.0198	.1571	38
.9800	.2400	.3000	.9137	.0319	.2163	21
.9800	.2600	.2800	.8954	.0279	.1749	26
.9800	.2800	.2400	.9128	.0389	.2138	24
.9800	.3600	.1400	.9370	.0858	.3041	13
.9800	.5000	.0600	.9477	.1915	.3704	11
.9800	.5400	.0400	.9578	.2834	.4645	9
.9800	.5600	.0600	.9114	.1275	.2107	19
.9800	.6600	.0200	.9538	.3849	.4231	12
.9800	.7400	.0200	.9085	.2685	.2042	17

whose solution furnishes an update of the design vector, i.e. $\kappa^{new} = \kappa^{old} + \Delta\kappa$, $\mu^{new} = \mu^{old} + \Delta\mu$ and $v_2^{new} = v_2^{old} + \Delta v_2$. The procedure is repeated iteratively. In theory, for a given target desired micro–macro response, there can be multiple feasible solutions. This is in part due to the structure of π^2 as well as the concave dependence of the Hashin–Shtrikman bounds on the mismatch and their convex dependence on the volume fraction (Figure 5). A general closed-form a priori criterion to predict the occurrence of multiple feasible solutions, or possibly no solutions (like the expressions in Equation 8 for one dimension), is at present lacking.

Pertaining to CASE I, depicted in Table 1 are all feasible designs between $1 < \frac{\kappa_2}{\kappa_1} < 10$, $1 < \frac{\mu_2}{\mu_1} < 10$ and $0 < v_2 < 0.5$, which deliver desired micro–macro responses between $1 < \frac{\kappa^{*,D}}{\kappa_1} < 10$, $1 < \frac{\mu^{*,D}}{\mu_1} < 10$ and $0 < \delta < 1$. For CASE II, All designs between $0 < \frac{\kappa_2}{\kappa_1} < 1$, $0 < \frac{\mu_2}{\mu_1} < 1$ and $0 < v_2 < 0.5$, which deliver desired micro–macro responses

between $0 < \frac{\kappa^{*,D}}{\kappa_1} < 1$, $0 < \frac{\mu^{*,D}}{\mu_1} < 1$ and $0 < \delta < 1$ are shown in Table 2. For each case, $\frac{\kappa^{*,D}}{\kappa_1}$, $\frac{\mu^{*,D}}{\mu_1}$ and δ were specified, and $\frac{\kappa_2}{\kappa_1}$, $\frac{\mu_2}{\mu_1}$ and v_2 were determined. In each case κ_1 and μ_1 were fixed. The external loading was $\mathcal{E}_{ij} = 0.001$, $i,j = 1,2,3$, or equivalently $\mathcal{L} = \mathbb{R} : \mathcal{E}$. Consistent with the observations for the one-dimensional example, there can be unattainable micro–macro objectives (infeasible goals). This was determined by the lack convergence characterized by Newton's algorithm being unable to meet a residual convergence criterion, $r \stackrel{\text{def}}{=} \sqrt{(\frac{\kappa^*}{\kappa^{*,D}} - 1)^2 + (\frac{\mu^*}{\mu^{*,D}} - 1)^2 + (\pi - \delta)^2} < 10^{-8}$, in 1000 iterations or less for a given starting vector. All searches were started at $v_2 = 0.5$, $\kappa_2 = \kappa^{*,D}$ and $\mu_2 = \mu^{*,D}$. We remark that to test over 125,000 design specifications, which corresponds to partitioning $0 < \frac{\kappa^{*,D}}{\kappa_1} < 1$, $0 < \frac{\mu^{*,D}}{\mu_1} < 1$ and $0 < \delta < 1$ into 50 increments in each interval direction, a $50 \times 50 \times 50$ 'design grid', each time solving an entire Newton search for the corresponding microstructural design (κ_2, μ_2, v_2), took no more than 30 seconds on a single workstation (IBM RISC 6000 series). The numerical simulations found no feasible microstructures for hard-matrix/soft-particle combinations where the bulk and shear mismatches were roughly the same (Table 2). This is consistent with the theoretical predictions indicating rapid growth in the microfield distortion for this case.

6. CONCLUSIONS

The potential residual, π^2, provides easily accessible information about the magnitude of the distortion of the microstress and microstrain fields, defined as the difference, in an induced energy norm, between the fields produced when heterogeneities are present and the fields produced when the heterogeneities are absent. This result was obtained under no assumptions on the character of the inhomogeneous material microstructure, other than that it be pointwise positive-definite. The usefulness of the potential residual lies in the fact that it is solely in terms of the external loading and accessible microstructural data, such as the properties of the constituents and their respective volume fractions. Therefore, the determination of the potential residual requires no extra significant computational effort. The use of π^2 in material design and development, in conjunction with approximate, computationally inexpensive, effective property estimates, permits one to account for the microfield distortion in the design of the macroscopic behavior of a multiphase material. As illustrated in the examples, this allows one to narrow down the number of microstructural designs which have appropriate microstructural behavior without resorting to intensive microscale simulations. Afterwards, more precise analyses of the responses can be performed, *on a reduced set of feasible designs*, employing intensive large-scale numerical techniques or laboratory experiments.

NOTES

1. For example for particulate materials, parameters such as volume fractions, mechanical properties and topologies of the second phases to add to a homogeneous base matrix might be sought.
2. The incorporation of the potential residual is general, and could be used with any desired effective property approximation method.

7. REFERENCES

[1] Huet, C.: Application of variational concepts to size effects in elastic heterogeneous bodies. *J. Mech. Phys. Solids*, 38, 813–841 (1990).

[2] Zohdi, T. I., Wriggers, P. and Huet, C.: A method of substructuring large-scale computational micromechanical problems. *Computer Methods Appl. Mech. Eng.*, at press (2002).

[3] Huet, C.: An integrated micromechanics and statistical continuum thermodynamics approach for studying the fracture behaviour of microcracked heterogeneous materials with delayed response. *Eng. Fracture Mech*., 58 (Special Issue 5—6), 459-556 (1997).

[4] Huet, C.: Coupled size and boundary condition effects in viscoelastic heterogeneous bodies. *Mech. Mater*., 31, 787–829 (1999).

[5] Nemat-Nasser, S. and Hori, M.: *Micromechanics: Overall Properties of Heterogeneous Solids*, 2nd edn, Elsevier, Amsterdam, 1999.

[6] Eshelby, J. D.: The elastic field of an ellipsoidal inclusion, and related problems. *Proc. R. Soc*., A 241, 376–396 (1957).

[7] Hashin, Z. and Shtrikman, S.: On some variational principles in anisotropic and nonhomogeneous elasticity. *J. Mech. Phys. Solids*, 10, 335–342 (1962).

[8] Hashin, Z. and Shtrikman, S.: A variational approach to the theory of the elastic behaviour of multiphase materials. *J. Mech. Phys. Solids*, 11, 127–140 (1963).

[9] Budiansky, B.: On the elastic moduli of some heterogeneous materials. *J. Mech. Phys. Solids*, 13, 223–227 (1965).

[10] Hill, R.: A self-consistent mechanics of composite materials. *J. Mech. Phys. Solids*, 13, 213–222 (1965).

[11] Mori, T. and Tanaka, K.: Average stress in matrix and average energy of materials with misfitting inclusions. *Acta Metall.*, 21, 571–574 (1973).

[12] Hill, R.: The elastic behaviour of acrystalline aggregate. *Proc. Phys. Soc. Lond.*, A 65, 349–354 (1952).

[13] Voigt, W.: Über die Beziehung zwischen den beiden Elastizitätskonstanten isotroper Körper. *Wied. Ann.*, 38, 573–587 (1889).

[14] Reuss, A.: Berechnung der Fliessgrenze von Mischkristallen auf Grund der Plastizitätsbedingung für Einkristalle. *Z. Angew. Math. Mech.*, 9, 49–58 (1929).

[15] Zohdi, T. I.: Overall solution-difference bounds on the effects of material inhomogeneities. *J. Elasticity*, 58, 249–255 (2000).